BIOPHYSIQUE À L'ÉCHELLE DE LA MOLÉCULE UNIQUE
SINGLE-MOLECULE BIOPHYSICS

Tracking enzymatic steps of DNA topoisomerases using single-molecule micromanipulation

Terence R. Strick [a], Gilles Charvin [b], Nynke H. Dekker [b], Jean-François Allemand [b], David Bensimon [b], Vincent Croquette [b]*

[a] Cold Spring Harbor Labs, Beckman Building, 1 Bungtown Road, Cold Spring Harbor, NY 11724, USA

[b] Laboratoire de physique statistique et département de biologie de l'École normale supérieure, UMR 8550 CNRS, associated with the Universities of Paris VI and Paris VII, 24, rue Lhomond, 75231 Paris cedex 05, France

Abstract   In this article, we describe single-molecule assays using magnetic traps and we applied these assays to topoisomerase enzymes which unwind and disentangle DNA molecules. First, the elasticity of single DNA molecule is characterized using the magnetic trap. We show that a twisting constraint may be easily applied and that its effect upon DNA may be measured accurately. Then we describe how the topoisomerase activity may be observed at the single-molecule level giving direct access to the important biological parameters of the enzyme such as velocity and processivity. Furthermore, individual cycles of unwinding can be observed in real time. This permits an accurate characterization of the enzyme's biochemical cycle. The data treatment required to identify and analyze individual topoisomerization cycles will be presented in detail. This analysis is applicable to a wide variety of molecular motors. *To cite this article: T.R. Strick et al., C. R. Physique 3 (2002) 595–618.* © 2002 Académie des sciences/Éditions scientifiques et médicales Elsevier SAS

micromanipulation / magnetic tweezers / topoisomerases

Observation des cycles enzymatiques des ADN topoisomérases par micromanipulation de molécules individuelles

Résumé   Dans cet article, nous décrivons des expériences sur des molécules individuelles utilisant des pinces magnétiques. Nous les utilisons pour caractériser les enzymes topoisomérases dont le rôle biologique est de démêler les molécules d'ADN. Dans un premier temps, l'élasticité d'une molécule d'ADN est mesurée en utilisant cette technique de micromanipulation. Nous montrons qu'il est facile de contrôler une contrainte de torsion sur une molécule d'ADN et que son effet sur son élasticité peut être mesuré avec précision. Nous décrivons ensuite l'observation de l'activité enzymatique à l'échelle de la molécule unique. Ceci nous permet d'accéder à la mesure des constantes réactionnelles de l'enzyme tel sa vitesse ou sa processivité. Nous passons en revue les résultats que nous avons obtenus en particulier sut la topoisomérase II, et nous montrons qu'il est possible d'enregistrer en temps réel les cycles de déroulement d'une molécule d'ADN sous torsion. Ceci nous permet une caractérisation précise de la biochimie de cette enzyme. La mesure directe des cycles enzymatiques ne peut se faire que lorsque le rapport signal sur bruit du dispositif expérimental est élevé.

---

* Correspondence and reprints.

E-mail addresses: strick@cshl.org (T.R. Strick); gilles.charvin@lps.ens.fr (G. Charvin); nynke.dekker@lps.ens.fr (N.H. Dekker); allemand@lps.ens.fr (J.-F. Allemand); david.bensimon@lps.ens.fr (D. Bensimon); vincent.croquette@lps.ens.fr (V. Croquette).

Nous discutons également les méthodes de traitement des données qui permettent d'accéder à la distribution des cycles enzymatiques en fonction de la qualité du rapport signal sur bruit. *Pour citer cet article : T.R. Strick et al., C. R. Physique 3 (2002) 595–618.* © 2002 Académie des sciences/Éditions scientifiques et médicales Elsevier SAS

micromanipulation / pinces magnétiques / topoisomerases

Acronyms and definitions

dsDNA (double stranded DNA): the helical molecule formed by two complementary single-stranded DNA.

ssDNA (single stranded DNA).

AFM (Atomic Force Microscopy): special microscope derived from the Scanning Tunneling Microscope. A sharp tip is scanned above the surface of interest while the applied force is servo to remain constant.

ATP (Adenosine Tri-Phosphate): one of the nucleic acids (adenosine) involved in the ARN. It is in the high energy three phosphate form. It hydrolysis fuels nearly all enzymatic activity.

F_1-ATPase (the enzyme sub-unit F_1-ATPase): sub-unit F1 of the enzyme in charge of producing ATP from its lower energy components: Adenosine Di Phosphate (ADP) and Phosphate.

kinesin (the kinesin molecular motor): a motor protein which moves along microtubules. This protein is very processive. It typically transports small vesicles over long distances in the cell (in the neurones, for instance. For further information see http://www.blocks.fhcrh.org/kinesin/index.html).

microtubules (microtubule filament protein): a globular protein made of two sub-units which assembles in a tubular form creating a very rigid filament involved in many cellular processes.

myosin (the myosin molecular motor): a motor protein family associated with the action filament. Myosin II is a major component found in muscle and responsible for contraction (more information may be found at: http://www.mrclmb.cam.ac.uk./myosin/myosin.html).

Topo II (Topoisomerase II): an enzyme which can modify DNA topology by forming a transient break in the double helix while passing neighboring DNA through the break.

BFP (biomembrane force probes): a force sensor introduced by E. Evans [10] based on the attachment of either a red blood cell or a phospholipid vesicle hold at the tip of a micropipette under a slight depression. The stiffness of this sensor can be evaluated directly from the depression and the measure of the diameters of the pipette-tip and the vesicle.

plasmid: a circular DNA molecule.

supercoiling: the result of adding or removing a torsional constraint to a DNA molecule or to a tube.

writhe: supercoiling partition in two forms: (1) twist and (2) writhe corresponding to inter-wound structures.

plectoneme: the inter-wound structure which appears on a supercoiled molecule or a telephone cord.

nick: single-stranded break in a double-stranded DNA molecule. A nick can act as a swivel to relax supercoiling in a DNA molecule.

Topo IV (Topoisomerase IV): an enzyme which can modify DNA topology in a process similar to that of Topo II. However Topo IV does relax well negative supercoiling and is adapted to disentangle DNA molecules.

gyrase: a prokaryotic topoisomerase which unwinds DNA molecules in bacteria.

biotin (biotin molecule): a small molecule also called Vitamin H. It is the paradigm of the key in the key-lock (ligand–receptor) model of molecular binding.

steptavidin (steptavidin molecule): a protein having four cavity presenting a tremendous affinity with biotin. It is the paradigm of the lock in the key-lock (ligand–receptor) model of molecular binding.

FJC (Freely Jointed Chain): the simplest polymer model which describes the molecule as a series of independent monomers.

WLC (Worm Like Chain): the simplest polymer model which describes the molecule as a flexible tube (or worm).

1. Introduction

A logical step following the recent achievement of genome sequencing is the understanding of the function of the coded genes. The study of the enzymes encoded by these genes, a major goal of post-genomic research, remains a challenging task. A complete understanding of enzymatic activity in the cell requires the measurement of both physical and chemical properties of these molecules.

Most enzymes are sophisticated catalysts that control the kinetics of the chemical reactions necessary for cell life. The study of their reaction pathways is usually realized in a test tube, involving large numbers of both enzyme and substrate. We shall refer to these methods as ensemble experiments. However, as revealed by their crystal structures, enzymes are extremely sophisticated nano-machines; thus ensemble experiments may not be sufficient to fully characterize their mechanisms.

Contrary to the static picture obtained by X-ray diffraction, in many cases the chemical reaction is achieved through an enzymatic cycle involving a structural change in the protein. Directly observing such events long remained a *gedanken experiment*, yet recent single-molecule studies have made this dream accessible. The most striking examples are the recent studies of linear molecular motors by Block et al. (kinesin) [1] and Spudich et al. (myosin) [2] and of rotary molecular motors by Kinosita and his colleagues (F1-ATPase) [3].

In this article we describe the use of a simple magnetic micromanipulator to study type II topoisomerases, which disentangle and unwind DNA molecules. We shall first show that single-molecule experiments are well-adapted to characterization of their enzymatic activity, recovering results obtained previously in ensemble experiments. We shall then demonstrate that single-molecule assays provide further information inaccessible to ensemble experiments. In particular, they offer the opportunity to observe enzyme activity in real time and to visualize individual enzymatic cycles. The analysis of enzymatic cycles reveals a cascade of chemical reactions obeying the rules of statistical physics. The statistical distribution of the cycling times may follow a simple Poisson distribution when there is a single rate-limiting step in the enzymatic reaction or it may show the existence of several rate-limiting steps. The ability to apply external constraints to the enzyme permits us to vary the enzymatic rate and to infer the nature of the rate-limiting step.

Access to such information is possible thanks to the high sensitivity of micro-manipulation techniques. To start, we briefly present the experimental apparatus. We discuss the force-measuring technique and the detection of individual enzymatic steps buried in experimental noise. Although our apparatus is sensitive, single enzymatic steps are small and the detection of these requires a critical analysis of their signal-to-noise. We then discuss the experimental measure of the DNA elasticity and its utility in verifying the attachment of a single DNA molecule. Next we describe the elasticity of a twisted DNA molecule. Finally, we apply these techniques to the study of topoisomerases.

2. Experimental micro-manipulation technique

2.1. The apparatus

The discovery of experimental sensors capable of detecting the forces applied by a single-molecule have opened the field of single-molecule micro-manipulation. Examples of such sensors include:
(1) the Atomic Force Microscopy (AFM), capable of exerting strong stretching forces on a fast time scale [5,6];
(2) optical tweezers (OT) [7], extremely sensitive and convenient [8,9];
(3) biomembrane force probes (BFP), which offer a simple and easily calibrated tunable sensor [10,11]; and
(4) magnetic tweezers, which were the first sensor used to study the stretching of a single DNA molecule [12].
A discussion of these various experimental approaches may be found in [13]. In this paper, our focus will be on magnetic tweezers.
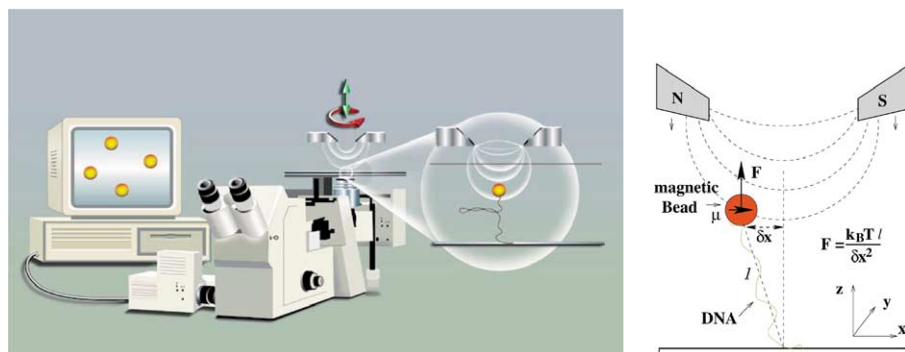
Figure 1. Left: experimental setup used to micro-manipulate a single DNA molecule. The DNA is attached to the bottom of a small capillary tube at one end and to a magnetic bead at the other end. We can pull and twist this molecule using small magnets placed above the capillary. The position of the magnetic bead is measured using an inverted microscope placed below the capillary. The 3D position of the bead is analyzed at video rates by computer software. (This image was drawn by Biofutur [4].) Right: principle used to measure the stretching force acting on the DNA molecule. The bead and the molecule behave like a small pendulum, the stiffness of which is evaluated through the magnitude of the bead's Brownian motion.

To study the activity of enzymes working on DNA, we have developed a single DNA micromanipulation assay which allows one to twist a single DNA molecule [14,15]. In this assay, DNA molecules are multi-labeled with biotin at one end and digoxigenin at the other end. The DNA is then incubated with magnetic beads coated with streptavidin. Next, we introduce these beads into a glass capillary (50 mm $\times$ 1 mm $\times$ 1 mm) coated with antidigoxigenin. We image the magnetic beads through the bottom surface of the capillary using an oil-immersion objective. Finally, forces are applied using rare earth magnets providing a horizontal magnetic field with a strong vertical gradient just above the observation area (see Fig. 1).

Using this experimental setup, we are able to apply well-defined stretching and twisting constraints to the DNA molecule while monitoring its extension. The tethered magnetic beads are pulled vertically with a force F that is easily controlled by adjusting the distance between the magnets and the beads. Rotating the magnets about the vertical axis offers the ability to rotate the beads and thus to twist the molecule at constant force. If the molecule is an intact double helix, the twisting constraint increases with magnet rotation provided DNA is anchored to the bead and the capillary at multiple points. We are thus able to apply a variable degree of torsion constraint n to a single DNA molecule.

2.2. Force measurement

We have developed a force measurement technique which relies upon measurement of the thermal Brownian fluctuations of the bead to accurately determine the force applied to the DNA molecule [14]. The system, consisting of small bead pulling with a force F on the molecule of length l is equivalent to a small, inverted vertical pendulum whose stiffness k is given by F/l. Measurement of the horizontal fluctuations of the bead δx, δy allows us to calculate this stiffness using the equipartition theorem: $k_B T = (F/l)\delta_{x \text{ or } y}^2$. We use a video camera connected to a frame grabber and a real-time data treatment algorithm to measure the fluctuations δx, δy of the bead with a resolution of ~ 10 nm. The diffraction ring pattern of the bead observed with parallel illumination is used to measure the vertical position of the bead in real time with a resolution of ~ 10 nm [16].

2.3. Intrinsic experimental noise

What is the ultimate limit in measuring enzymatic activity on a single DNA molecule? Since we can only detect the enzymatic activity through changes in DNA extension, our sensitivity is limited by the noise level imposed by the Brownian fluctuations of the bead.

We can estimate this noise level x_n by modeling our molecular assay as a spring of stiffness k linked to a bead of radius r_b having a viscous drag coefficient $6\pi\eta r_b$. This last term is dissipative in nature and is thus responsible for the noise level through the so-called Langevin force $F_L = \sqrt{4k_B T \cdot 6\pi\eta r_b}$. The order of magnitude of this intrinsic force noise is $10\ fN/\sqrt{Hz}$ for a micron-sized bead. To convert this force noise into displacement noise we divide it by the molecule's stiffness k yielding $x_n = F_L/k$. This noise may be reduced by decreasing the length of the DNA molecule (hence increasing k) or by decreasing the size of the bead r_b (hence decreasing the dissipation).

However, the maximum force that can be applied to a magnetic bead is proportional to the cube of the bead's radius. In our magnet configuration this implies that the bead radius cannot be reduced to a value significantly below 0.5 μm. The effective stiffness k of a 10 kilo-base (kb) molecule stretched by 1 pN is in the range of 10^{-6} N/m. Thus in these conditions, the typical fluctuations of the molecule's extension are $10\ nm/\sqrt{Hz}$.

2.4. Measuring the enzymatic step size and building the probability distribution of enzyme activity in a noisy signal

Many single-molecule experiments consist of measuring a series of consecutive noisy steps of fixed size ϵ. For example, kinesin proceeds along microtubules in 8 nm steps [17]; the F1-ATPase system executes rotational steps of 120° [18]; type II topoisomerases (Topo II) relax supercoiled DNA by 2 turns per cycle (discussed in detail below).

The interest of these experiments lies in their ability to directly observe the step size of the motor enzyme, and resolve each enzymatic cycle. Then we can extract the probability distribution of enzyme activity, i.e. the distribution of times between steps. This provides crucial information about the kinetic properties of the motor. However, the measured signal (a linear or rotational displacement of a microscopic sensor, usually a small bead) may be accompanied by a large amount of white noise due to the Brownian motion of the sensor, making it difficult to distinguish enzymatic steps in the time domain.

We discuss below two approaches to characterize the probability distribution, one in real space and its counterpart in Fourier space [19] (The Fourier method relies upon the different statistical behavior of power spectra for signal and noise). A convenient way of observing the statistical nature of enzymatic behaviour has been proposed by Block et al. [9,20]. By considering that an enzymatic cycle is composed of series of simple poissonian kinetic steps, they have shown that the probability distribution of enzymatic activity can be fully characterized by the randomness parameter, the ratio r between the variance and the mean of the number of steps of size ϵ for a signal of duration T:

$$r = \frac{(z - \langle z \rangle)_T^2}{(\epsilon \cdot \langle z \rangle)_T}, \tag{1}$$

where z is the variable used to quantify the steps. Then, if there are p limiting kinetic steps in the enzymatic cycle, it can be shown that:

$$r = \frac{1}{p}. \tag{2}$$

If the enzymatic process is Poissonian $r = 1$, whereas $r = 0$ for a clock-like motor.

2.4.1. *Characterization of enzymatic activity in the frequency domain*

The analysis of enzymatic signal leads to ask two simple questions: how much information can be retrieved from the noisy background during an experiment? How is this information to be extracted?

The best way to answer the first question is to look at the signal properties in the frequency domain, because the spectral analysis provides a quantitative criterion to characterize the signal/noise ratio [19].

The ideal signal (without noise) for a processive enzyme, a series of steps of equal height but variable duration (Poisson distribution), has a $1/f^2$ frequency spectrum corresponding to the average of the uncorrelated Fourier transforms of individual Heaviside functions. In experiments, this ideal signal is superimposed upon the white noise of the detector. The signal (A/f^2 in the frequency domain) equals the noise level D at a critical frequency $f_c = \sqrt{A/D}$. All the information regarding enzymatic activity is localized between $f_T = 1/T$, the lowest observable frequency for a run of duration T, and f_c. The quality of the data is thus reflected in the ratio $Q = f_c/f_T$.

If $Q < 1$, noise overcomes the enzymatic signal at all observable frequencies and no information can be extracted. If $Q > N$, where N is the number of steps occurring during T, then $f_c > N/T$, the stepping frequency N/T of the motor is smaller than the critical frequency, and steps are recognized in the temporal signal. Then, real time averaging techniques (Section 2.4.2) can be used to measure probability distribution and measure the step size of the motor. In the intermediate regime, if $1 < Q < N$, steps cannot be identified in the time domain but their size ϵ can be deduced from a measurement of A using the relationship:

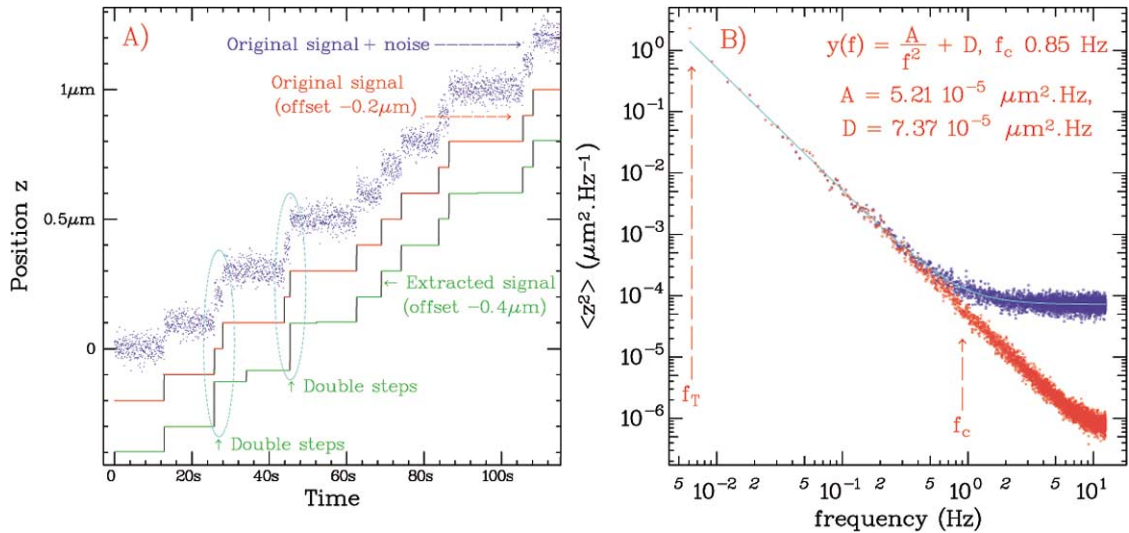$$A = \frac{\epsilon v}{2\pi^2},\qquad(3)$$

Figure 2. Data analysis of a noisy step signal. (A) Simulated enzymatic signal (blue trace) built with a stair-like signal (red trace) added to a Gaussian noise (0.03 μm in magnitude). The idealized enzymatic signal (red) presents a series of steps of 0.1 μm in height with a Poisson distributed duration of ~ 5 s characteristic time (the red curve has been offset by -0.2 μm from the blue one). The green curve is obtained by processing the blue curve with the step extracting algorithm described in Section 2.4.2. The green curve has been offset by -0.2 μm from the red one. If the algorithm was perfect, the green curve should coincide with the red one. However, the extra noise alters this process, the major discrepancies appearing when two steps are separated by a very short period (which is allowed by the Poisson distribution). In this case, the algorithm finds double steps (see the cyan ellipses). (B) Power spectrum analysis of the blue and red signals averaged with signal having the same property to increase the signal to noise ratio. The pure step signal leads to a $1/f^2$ spectrum, the noise is responsible of the high frequency behavior. By measuring the A/f^2 component, we can access the step-size and/or the step distribution statistic leading to $\epsilon = 0.103$ μm while the exact value is 0.1 μm. The quality factor $Q = f_c/f_T \sim 140$ is larger than the number of steps in the time window (see Section 2.4.1).

where v is the enzymatic mean rate and we assume the stepping statistics to follow Poisson statistics. However, when the distribution deviates from Poisson, this relationship becomes:

$$\lim_{f \to 0} A = \frac{r \epsilon v}{2\pi^2}, \tag{4}$$

where r is the randomness parameter introduced above. Thus if one knows the value of the step size ϵ one can compute r and characterize the probability distribution, even if steps are not visible in the time domain.

2.4.2. *Characterization of enzymatic activity in the time domain*

In case of high signal to noise ratio, which is characterized by $Q > N$, we can determine the enzyme's steps in the time domain (our detailed algorithm for distinguishing step signal from noise is described in the appendix). In short, we fit our data to a series of steps of arbitrary size and duration, with minimum time interval limited to an averaging time $t_c = 1/f_c$. A simulated enzymatic signal and its data treatment is shown in Fig. 2. Real records of enzymatic activity are discussed in Section 4.4.3.

3. Elastic properties of the DNA molecule

We will now describe the mechanical response of DNA to stretching and twisting. In our experiments we typically change one of these two parameters at a time and measure the resulting end-to-end extension z of the DNA.

3.1. Stretching a single DNA molecule

For each bead studied, we first verify that it is linked to the glass surface by a single-molecule by recording the force extension curve and comparing it to the Worm Like Chain model [21,22] known to accurately describe the elastic behavior of DNA (see Fig. 3) at forces up to 10 pN. (For higher forces, this elastic behavior presents a sharp structural transition leading to a strong overstretching of the molecule [23,24].) Finding a value of the persistence length L_p in the range of 50 nm attests that we are stretching a single DNA molecule.

3.2. Twisting the DNA molecule

DNA supercoiling has been extensively studied because it links the biological activity of DNA to its tertiary structure. These studies here focussed on the sequencing of circular loops of DNA (plasmids). Boles et al. [25] and Bednar et al. [26] have studied electrophoretic gel-mobility shift assays to characterize the properties of their topoisomers. The topology of such torsionally constrained molecules can be described

Figure 3. Experimental data and fit corresponding to the extension of a λ-DNA molecule in 10 mM phosphate buffer obtained using the Brownian motion method. The logarithmic scale demonstrates the large force range covered by the technique. The WLC model (full line) fits very nicely the experimental data. As a comparison we have also drawn the prediction of the Freely Jointed Chain (FJC) model with the same persistence and contour lengths.
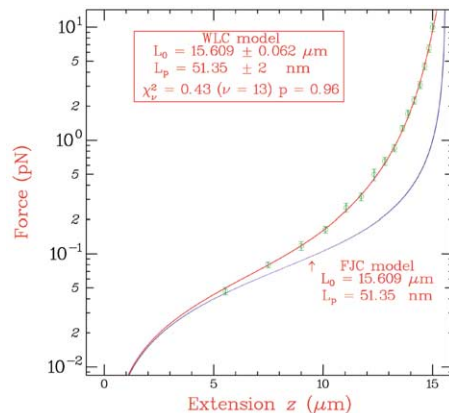
by a few simple quantities [27,28]. For a given molecule, its supercoiling may be characterized by the number of turns n added to or removed from its relaxed state. Since DNA is a right handed double helix, in its relaxed form the two strands of DNA wind around each other by Lk_0 turns, where Lk_0 is called the linking number of the molecule. Twisting the molecule by n turns will either increase or decrease this linking number $Lk = Lk_0 + n$. We shall describe below the effect of these extra turns. Although we shall mainly use the variable n to describe the supercoiling of a molecule, this variable cannot be used directly to compare the topology of two molecules of different length. The traditional variable used for that purpose is $\sigma = n/Lk_0$. We predominantly utilize n since the enzymes studied will alter this number by integer values. However, we shall plot curves with both variables whenever this is possible.

Much of the elastic behavior of coiled DNA can be understood by analogy with twisting a rubber tube under a stretching force F, see Fig. 4. When one begins to twist such a tube, its extension initially remains unchanged and the constraint accumulates as pure torsion. The torque applied to the tube Γ increases linearly with the twist angle $\Omega = 2\pi n$: $\Gamma = \frac{\mathcal{C}}{l_0}\Omega$ and its twist energy increases quadratically:

$$E_{\text{torsion}} = \frac{1}{2}\frac{\mathcal{C}}{l_0}\Omega^2,$$

where $\mathcal{C}$ is the tube's twist stiffness (usually written in the DNA context in units of $k_B T$: $\mathcal{C} \equiv k_B T C$).

As one continues to twist the tube, one notes that after a certain number of turns n_b (corresponding to a torque $\Gamma_b = 2\pi n_b \mathcal{C}/l_0$) the system buckles and a loop of radius R is formed. Alternatively it is said that the writhe is building up in the tube. The twist energy is thus transferred into bending energy and the work done against the stretching force F. Upon further twisting, the tube coils upon itself but the torque no longer increases (Fig. 4(B)). In spite of the stretching force F, the system's extension decreases by $2\pi R$ for every extra turn applied. Equating the torsional energy with the sum of the work done and the increase in bending energy, one obtains:

$$2\pi\Gamma_b = 2\pi RF + 2\pi R\frac{1}{2}\frac{B}{R^2}. \tag{5}$$
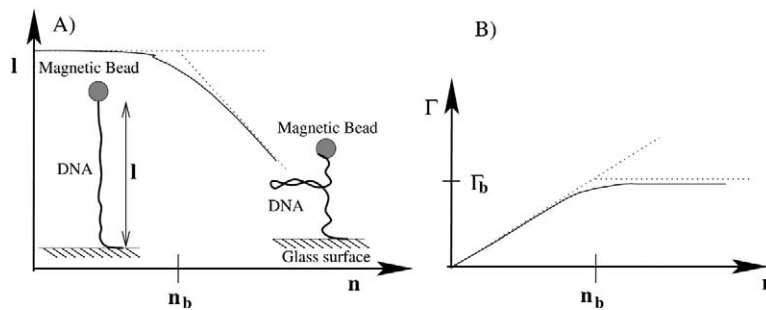

Figure 4. (A) The buckling instability of an elastic tube overwound by n turns and stretched by a constant force F is evidenced through the decrease of its extension l. Initially, the torsional constraint does not cause the system to contract. When $n = n_b$ turns have been applied to the tube, a buckling transition allows the system to relax its torsional constraint by forming a loop, causing the system to contract. As more twist is applied, the tube extension decreases linearly as the number of loops grows regularly. (B) Torque Γ acting on the tube as a function of the number of turns n. As long as the system remains extended, its torque increases linearly with the number of applied turns. When the critical torque $\Gamma = \Gamma_b$ is reached ($n = n_b$), the formation of a plectoneme relaxes the torsional constraint and prevents the torque from increasing beyond Γ_b. Each additional turn added to the system further lengthens the plectonemes, preventing the torque from increasing. The DNA molecule just behaves like this tube with a large level of fluctuations.
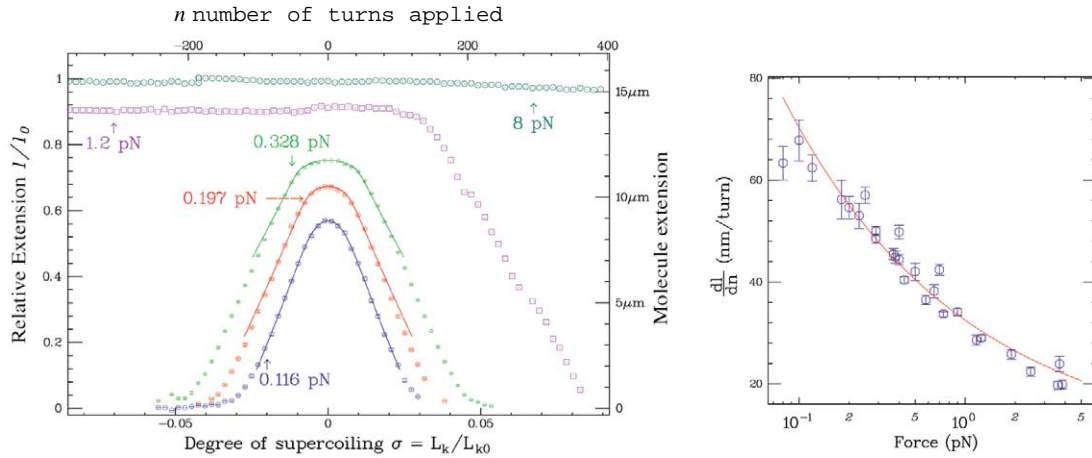
Figure 5. Left: relative extension l/l_0 of a DNA molecule versus its degree of supercoiling σ (converted to turns applied on the molecule on top scale) for various stretching forces. The curve done at $F = 1.2$ pN for positive supercoiling illustrates perfectly the buckling instability as described in the Fig. 4. The shortening of the molecule occurs at $n_b \sim 140$ turns. At lower forces, the instability threshold occurs very early and the behavior is symmetrical under $\sigma \to -\sigma$. The shortening corresponds to the formation of plectonemes upon application of writhe. For $F < 0.4$ pN the comparison between the experimental data (points) and the Rod-Like-Chain model with $C/k_B T = 86$ nm (full-line) is very good. The symmetry breaking observed at $F = 1.2$ pN is due to DNA denaturation [29]. At $F = 8$ pN the torque applied to the DNA induces structural transition both for negative and positive supercoiling [30]. Right: slope of the extension versus n curve after buckling as a function of force F. The continuous line is a fit with a power law dependence as $F^{-\alpha}$, with $\alpha = 0.4$. The naive mechanical model (see Section 3.2) yields $\alpha = 0.5$.

By minimizing this energy with respect to R, one finds that $2\pi F = \pi B/R^2$, or $R = \sqrt{B/(2F)}$ and $\Gamma_b = \sqrt{2BF}$. This implies that as the stretching force increases, the number of turns required for buckling n_b increases and the radius of the tube's coils (plectonemes) after buckling decreases.

This mechanical model qualitatively describes the behavior of supercoiled DNA (Fig. 5). In the purple curve obtained by overwinding DNA subjected to $F = 1.2$ pN, one can clearly identify the two regimes described above. For $n < n_b \sim 140$ the DNA's extension varies little, whereas for $n > n_b$ its extension decreases regularly. Moreover as F increases the slope dl/dn of the curves $l(n)$ decreases (see Fig. 5), as expected from the decrease of the plectonemic radius R with force. When we lower the stretching force F, the absolute value of the slope increases and n_b decreases. The strong and regular decrease in extension observed above n_b provides an accurate and simple means to measure the degree of supercoiling of a DNA molecule. A single turn applied to the molecule may easily be detected with a signal averaging of about one second.

The model just presented is of course over simplified. Typically, the buckling instability threshold is smeared by the strong thermal fluctuations. More accurate theoretical models, taking into account these fluctuations, agree well with experiments (Fig. 5) [21,31–35]. On the other hand, these elastic models break down when the twisting constraint on the DNA molecule becomes too large: if we unwind the molecule above a critical torque its double helical structure will melt [29,36]. Structural transitions are similarly induced following strong overtwisting [30,37].

4. Characterization of topoisomerases activity at the single-molecule level

We will first briefly present the current knowledge of topoisomerases prior to discussing the contribution of single-molecule experiments to their understanding. Then, we will illustrate the various issues of single-molecule assays on Topo II, in particular the criterion used to assess single enzyme activity. Next we
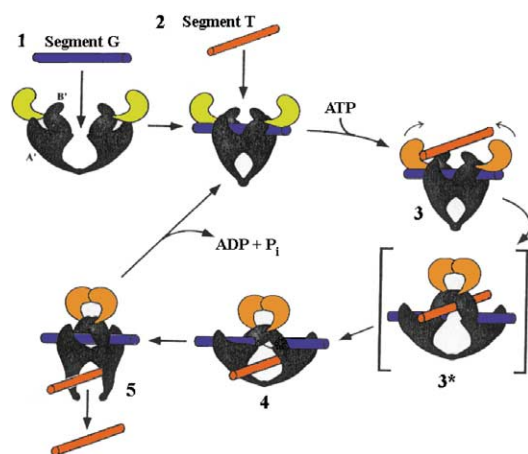
Figure 6. Rough sketch of the action of type II topoisomerases. They generate a double-strand break in the DNA, through which another DNA segment is transferred. Each enzymatic cycle causes $|\Delta Wr| = 2$. The cleaved segment is denoted G for 'gate', and the transported segment is noted T. (This picture is taken from [38].)

will present our results pertaining to the topoisomerase catalytic behavior: its processivity (the number of consecutive cycles) and its rate of supercoil removal. We will study the evolution of these parameters as a function of ATP concentration and analyze the statistics of individual enzymatic steps. Subsequently, we will show that single molecule assays can be used to detect the binding of an enzyme to DNA in the absence of ATP. Finally, by applying the same techniques to a prokaryotic homologous enzyme (Topo IV), we demonstrate that our setup is a powerful tool to study and compare the mechanism of these molecular motors.

4.1. Topoisomerases

Soon after the double helical structure was proposed for DNA [39], the replication of the circular DNA molecule of prokaryotic organisms raised an intriguing question: how did the two sister DNA molecules disentangle? This issue remained unsolved until the discovery of the topoisomerase family of enzymes by Wang [40]: these are ubiquitous enzymes capable of changing the topology of DNA molecules by cleaving one or both strands of DNA (type I and II topoisomerases, respectively) [41–45]. Topoisomerases are thus capable both of changing the degree of supercoiling in DNA molecules as well as affecting their degree of catenation.

Contrary to type II topoisomerases, type I topoisomerases (Topo I) do not require an energy cofactor (ATP) to transport a DNA segment through a transient single-stranded break in a second DNA segment [46]. Topo I is able to relax twisted DNA [47–49] or to change catenation provided the presence of a nick.

Based on the crystal structure [50] of a eukaryotic type II topoisomerase, the following mechanism was proposed to explain type II topoisomerase activity: (i) creation of a double strand break in one DNA segment (the gate G), (ii) transport of another DNA segment through the gate [50] (see Fig. 6), (iii) relegation of the gate segment. In this model the enzyme requires the consumption of two ATP molecules to perform its cycle.

However, the coupling between ATP consumption and mechanic activity, and more generally the kinetics of the enzymatic cycle are not fully understood. Our studies have tried to answer these fundamental questions by comparing the type II topoisomerases from a eukaryote (D.Melanogaster, Topo II) and a prokaryote (E.Coli, Topo IV). The rationale behind such a comparative study is that regulation of DNA topology in prokaryotes is expected to be different because of the topological constraint imposed by the circular chromosomes of prokaryote.

4.2. The single-molecule topoisomerase assay

Topoisomerases have been studied in ingenious ensemble experiments in which fixed twisting constraints are applied to circular DNA molecules (plasmids). However, such constraints are not easy to impose and
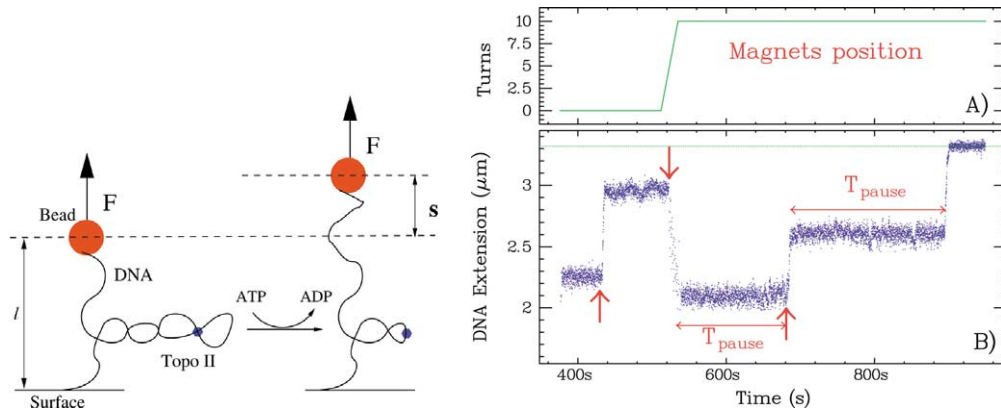
Figure 7. Left: relaxation of supercoils by topoisomerase II. By removing supercoils, the enzyme causes the DNA's extension to increase. Monitoring the system's extension during the course of the reaction makes real-time measurement of enzyme activity possible. Right: single-molecule characterization: the activity of topoisomerase II is recorded over time (B) in conditions where the ATP concentration is not limiting its rate ([ATP] = 300 μM). When the enzyme relaxes supercoils, the extension of the molecule rises (those events are associated to a rising arrow). These bursts of activity are separated by long pauses lasting minutes (T_{pause}). The molecule extension is reduced by switching on the magnets motors (see recording A and the arrow pointing downwards).

even more difficult to vary. These experimental difficulties disappear in our single-molecule assay, for DNA twisting is effected by simple magnet rotation. Provided that the stretching force F is not too high, the DNA molecule buckles and forms plectonemic supercoils. We monitor the molecule's extension z which characterizes the degree of supercoiling [14,15,29,30].

The rate of contraction $\delta = dz/dn$ for DNA depends on F as may be seen in Fig. 5 (at $F = 0.7$ pN in moderate salt we find that $\delta = 43$ nm/turn). To observe topoisomerase activity, a 10 kb dsDNA is coiled beyond the buckling threshold by spinning the magnets by typically 50 turns (corresponding to $\sigma \sim +0.05$). The enzyme, introduced in a proper buffer, will remove the inter-wound supercoils, thus leading to an increase in the molecule's extension. By mechanically winding the molecule again, we can re-form the supercoils and repeat the experiment (see Fig. 7).

4.3. Single-molecule criterion

Although there is only one dsDNA molecule present in the experiment, several enzymes may be active simultaneously. Working at the single-molecule level requires either the definition of a single activity site on the DNA molecule or very low enzyme concentrations. Since the structure of plectonemes offers multiple sites for Topo II activity, we have to rely on very low enzyme concentrations to guarantee single enzyme activity. Note that the typical concentration of enzyme in single molecule experiments is in the nM range which corresponds typically to one enzyme per μm³. As can be seen on Fig. 7(B), at low enzyme concentrations we observe no enzymatic activity for long period of times τ_{pause} that are separated by short bursts of activity on a time scale τ_{on}. When the ratio $\tau_{on}/\tau_{pause} \ll 1$ the probability that two enzymes act at the same time is exceedingly small. This is the criterion that we use to ensure that activity is at a single-enzyme level.

4.4. Topo II rate of activity and processivity

4.4.1. *Comparison with ensemble experiments*

Although our primary interest in single molecule experiments lies in extending the knowledge of enzymatic behaviour, it is logical to compare parameters obtained to those from ensemble experiments.

605

To compare our measurements with ensemble experiments, we have first determined the processive activity of a single Topo II enzyme on double-stranded DNA and verified that it follows Michaelis–Menten kinetics for both ATP and substrate (plectoneme) concentration.

Indeed the burst amplitudes give access to the enzyme processivity while their slope characterizes the enzymatic rate v. The bursts of activity correspond to a series of enzymatic cycles performed successively by a single enzyme. Successive completion of enzymatic cycles is typical of processive enzymes. For instance, the number of consecutive Topo II cycles performed at saturating ATP concentration and $F \sim$ 0.3 pN is a stochastic variable that follows a Poisson distribution with a mean value $\langle n \rangle \sim 15$ corresponding to the removal of about 30 supercoils.

By averaging different bursts of unwinding, see Fig. 8, the rate of activity of Topo II can be measured as a function of ATP concentration as shown in Fig. 9 (at a force of 0.7 pN). Fitting this curve to a Michaelis–Menten model [51] for the hydrolysis of ATP by Topo II:

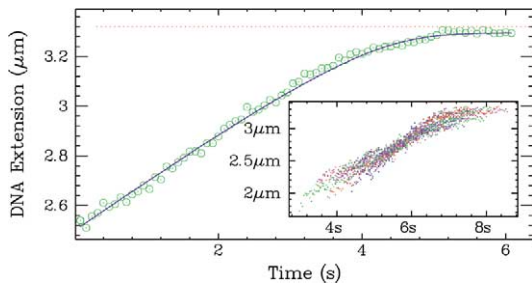$$V_{\max} = \frac{V_{\text{sat}}[\text{ATP}]}{K_m + [\text{ATP}]}, \tag{6}$$

Figure 8. Insert: superposition of about twenty relaxation curves obtained in the presence of 300 μM ATP. One notes that the variance in the curves is quite small. Main graph: Average of the curves shown in insert. The mean curve is characterized by a linear regime where the system's extension grows linearly, followed by a second regime where the extension tends asymptotically towards $l_{\max}$ (dotted line). The integral of the Michelis–Menten equation for the relaxation of supercoils (Eq. (7)) fits (solid line) the experimental data rather well.
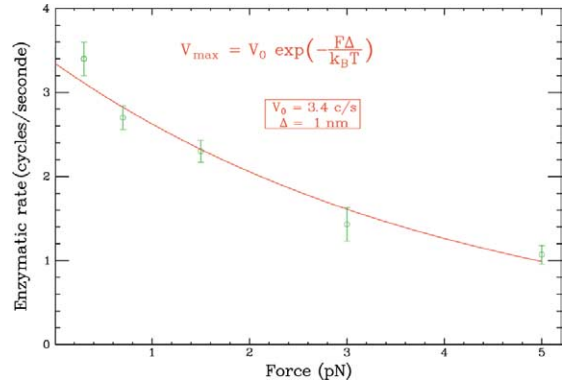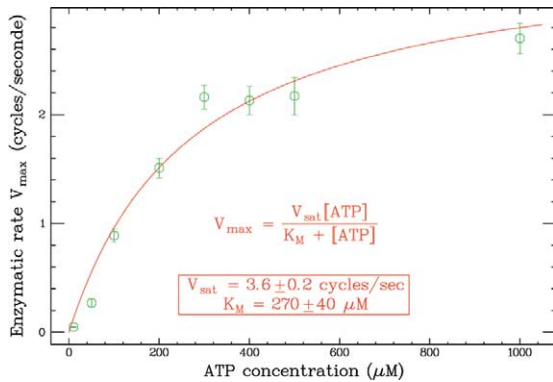

Figure 9. Left: maximal velocity of the reaction $V_{\max}$ as a function of ATP concentration. The data were obtained with a stretching force $F = 0.7$ pN. The error bars represent the statistical error in determining $V_{\max}$. By fitting the Michelis–Menten equation (6) to the experimental data, we obtain (solid line) the parameters shown in the plot.
Right: maximal velocity of the reaction $V_{\max}$ as a function of the stretching force applied to the DNA. The experiments were done in the presence of 1 mM ATP. The error bars represent the statistical error in the determination of $V_{\max}$. The continuous line is a fit of an exponential decay $V_{\max} = V_{\max}^0 \exp(-F\Delta/k_B T)$ to the experimental data (see text).

which yields $K_m = 270\,\mu M \pm 40$ and $V_{max} = 3.6 \pm 0.2$ turnovers per second, value consistent with ensemble data [51]: $K_m = 280\,\mu M$. Single-molecule assays give access to the true enzymatic rate whereas ensemble experiments yield a value that is averaged over active as well as inactive enzymes. The rate found in single-molecule assay (3 cycles per cycle at saturating ATP concentration for Topo II), turns out to be eight times larger than the one measured in ensemble [52]. This rate is compatible with the number of Topo II enzymes present in the cell required to unwind the two sister DNA molecules during replication.

Furthermore, we have measured the enzymatic rate versus the plectoneme concentration present on the DNA molecule. We observe that the rate of unwinding is independent of the degree of supercoiling until the number of supercoils n_w becomes of $O(1)$. Indeed the evolution of the rate of supercoil removal versus n_w can be described by Michaelis–Menten kinetics of order 1:

$$\frac{(l(0) - l(T))}{\delta} + k_{1/2} \log\left(\frac{l_{max} - l(T)}{l_{max} - l(0)}\right) = -V_{max}T, \tag{7}$$

with $n_{w_{1/2}} = 2$. These results ($n_{w_{1/2}} \sim 3$) are in agreement with ensemble measurements [51]. In other words, Topo II is extremely efficient at finding the DNA crossings present in supercoils, its substrate. This search becomes limiting when very few supercoils are left.

4.4.2. *Topoisomerase II is active on plectonemic dsDNA*

The buckling instability of a dsDNA molecule leads to a clear signal where the contribution of DNA to writhe n_w can be easily distinguished from its twist component n_t. In the experiment, we impose the linking number namely $L_k = n_w + n_t$. Since the extension reduction is proportional to n_w, n_t is easily deduced. This has helped us to determine the substrate of Topo II enzymes: Topo II is only active in the presence of writhe. To demonstrate this, we twisted the DNA by a fixed number of turns $n > n_b$. We have then introduced Topo II and ATP, waited several minutes so that the enzyme could relax the torsional constraint and rinsed the capillary to completely eliminate Topo II. We measured the residual twist of the molecule n_f and found it to be $\sim n_b$ (see Fig. 10). If Topo II acted on twisted molecules (without writhe), the residual twist should have been null. Our observations show that the enzyme is inefficient at relaxing twist in a DNA molecule below the buckling transition, i.e. in a regime where supercoils are energetically costly and improbable. When the stretching force F is increased, the threshold for buckling n_b increases and Topo II enzymes effectively cease to work at a higher residual twist.

Such a study is not possible in a ensemble experiment: a supercoiled plasmid in a test tube is not stretched by a force F. In such a system the buckling instability threshold n_b is equal to zero and twist and writhe always coexist. Hence in a test tube Topo II fully relaxes a supercoiled plasmid. In the single-molecule

Figure 10. The number of supercoils relaxed by Topo II decreases as the stretching force increases. The upwards arrows ($\uparrow$) indicate the initial degree of supercoiling of the DNA, and the downwards arrows ($\downarrow$) indicate the DNA's degree of supercoiling at the end of the reaction. n_f shows the number of turns for which the DNA buckles and begins to form plectonemes. Topo II relaxes just a few turns more than n_b.
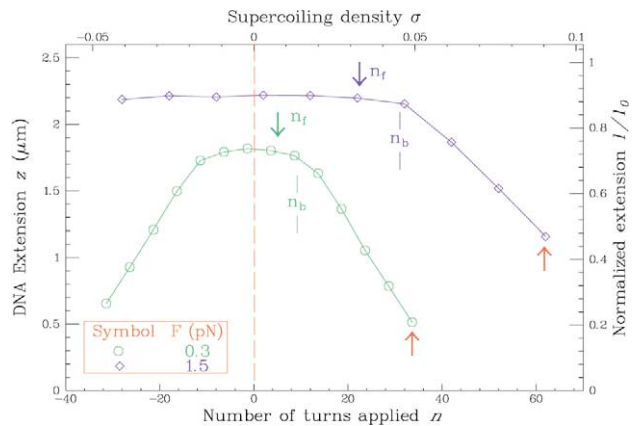
assay, the extra parameter provided by the stretching force F allows one to distinguish the enzyme's action on the two components of supercoiling: the twist and the writhe.

4.4.3. *Topo II relaxes both positive and negative supercoils with equivalent rates*

DNA supercoiling is not symmetrical with respect to rotation: positive supercoiling (adding turns to the double helix) stabilizes the dsDNA whereas negative supercoiling favors opening of the double helix. In spite of this asymmetry, it has been known for some time, that Topo II relaxes both positively and negatively supercoiled plasmids. To study the activity of Topo II on a negatively supercoiled DNA, we stretched it with a sufficiently low force (0.3 pN) such that unwinding did not locally denature the molecule. We measured the reaction rate V_{max} at saturating [ATP] (1 mM). We repeated the experiment on a similarly positively coiled molecule and did not detect a significant difference between the rate of relaxation of positive or negative supercoils: $V_{max}^{\sigma<0} = 2.6 \pm 0.2$ cycles/s and $V_{max}^{\sigma>0} = 3.4 \pm 0.2$ cycles/s.

4.4.4. *Influence of the DNA stretching force upon enzymatic cycles on Topo II*

The stretching force is observed to influence the enzymatic rate. For Topo II we have measured V_{max} as a function of F [53,17] ($0.3 \leqslant F \leqslant 5$ pN) on positively supercoiled DNA in saturating ATP conditions
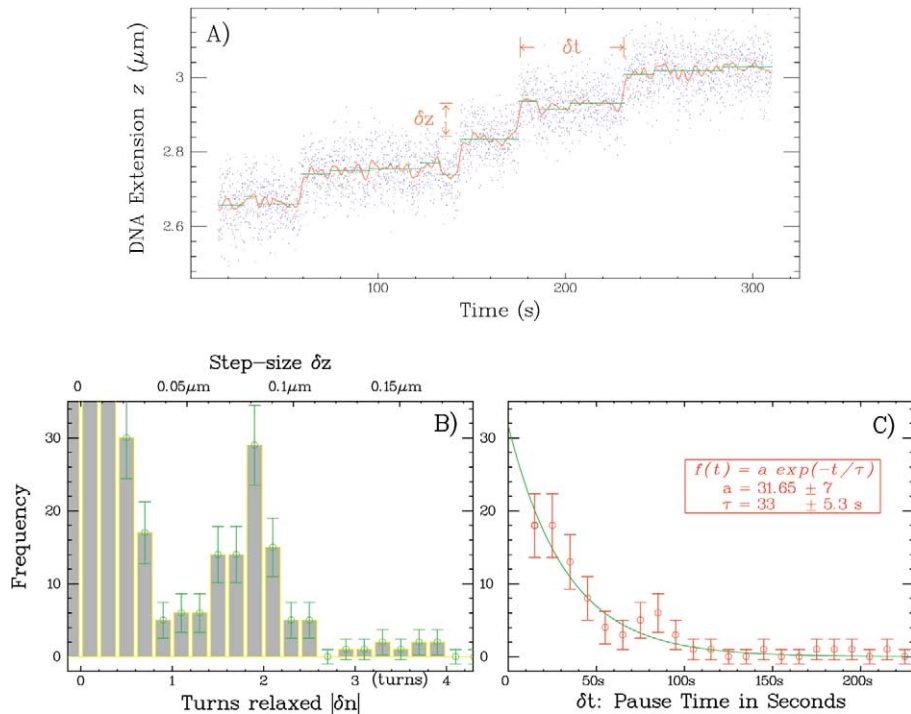

Figure 11. Relaxation of supercoils by Topo II in the presence of 10 μM ATP at $F = 0.7$ pN. (A) Measuring the extension of the system as a function of time $l(t)$ makes it possible to observe discrete steps in the system's extension δz lasting for δt. Blue points correspond to raw data obtained at 12.5 Hz, the full red line is a one-second average of the raw data. The green horizontal segments correspond to steps extracted by the algorithm describe in Section 2.4.2 with a minimum averaging time of 5 s. Over this timescale, the error on the system's extension due to the bead's Brownian fluctuations is on the order of 10 nm. (B) Histogram of distances δz for all significant steps (here 114) in curves (A) and similar. The peaks in the histogram confirm that the steps in curve (A) are separated by mean distances of 86 nm corresponding to $\Delta Lk = -2$. The noise may be estimated by the shoulder of the peak centered on $\delta z = 0$. (C) Histogram of the cycle duration δt corresponding to an exponential (Poisson) with a characteristic time $\tau = 33 \pm 6$ s ($n = 114$).

(1 mM). We observe that the turnover rate is decreased by a factor of three when we increase F from 0.3 to 5 pN. Our results imply that the enzyme performs work $F \cdot \Delta$ (with $\Delta \sim 1$ nm) against the force, with a consequent slowing down of its activity by an Arrhenius factor $\exp(-F\Delta/k_{\mathrm{B}}T)$ [53]. This suggests that closure of the cleaved DNA segment may be rate-limiting.

The rate of Topo II relaxation events may thus be influenced both by the applied external force and by the ATP concentration.

4.4.5. *Observation of individual enzymatic cycles of Topo II*

In order to observe individual enzymatic cycles of Topo II activity, we work at very low ATP concentration (10 or 20 µM) where the enzyme is sufficiently slowed down that individual relaxation events can be identified. The extension of the molecule increases as a function of time by well-defined steps of 86 nm (at $F = 0.7$ pN), corresponding to the simultaneous relaxation of two supercoils (see Fig. 11(A)). For a large number of experiments, the frequency of observed steps can be binned as function of their size as shown in Fig. 11(B). We observe a pronounced peak corresponding to the relaxation of two supercoils. We have further analyzed the time between steps (Fig. 11(C)) and found it to follow an exponential distribution. This is consistent with the burning of a single ATP per cycle [54], although we cannot rule out the hydrolysis of a second ATP [55,56] on a time-scale shorter than our temporal resolution: ~ 1 s.

As discussed above, the observation of individual steps requires averaging the signal over some time (or low-pass filtering) to reduce the experimental noise. Since the experimental noise increases when we lower the force F, it is more difficult to observe steps for negative supercoiling where the stretching force is limited to values smaller than 0.5 pN to avoid denaturation [57]. Increasing the ATP concentration reduces the enzymatic turnover time, which soon becomes smaller than the minimum averaging time required to distinguish steps. Thus, when [ATP] exceeds 50 µM, steps are no longer distinguishable.

4.5. Topo II binding events in the absence of ATP

We now completely deprive the enzyme of its energetic cofactor so that it may only explore the first few sub-states of its cycle. Indeed, in the absence of ATP Topo II is unable to change the linking number of DNA, although ensemble experiments indicate that in such conditions the enzyme is capable of clamping onto a crossover between two DNA segments [58,59]. In such a complex, the enzyme interacts with both DNA segments. Evidence for the DNA binding of Topo II is easily observed on an overwound single-molecule. The fluctuations of its extension are altered in the presence of the enzyme. The Lorenzian noise observed for these fluctuations in the absence of Topo II is transformed to a $\sim 1/f$-spectrum in the presence of Topo II. This simple test is however not easy to quantify and we present here two assays with simpler interpretations. We shall refer to the first method as the 'yanking assay' and and to the second one as the 'clamping assay'.

4.5.1. *Topo II firmly holds the two DNA segments*

To check the binding of Topo II to DNA crossings, we use the sensitivity of the buckling instability threshold n_{b} to the stretching force F. First a supercoiled molecule twisted by n turns at 1 pN leading to a significant reduction in its extension ($n > n_{\mathrm{b}}$ (1 pN)). When the force is increased to $F = 5$ pN, n_{b} increases drastically and exceeds n: the molecule does not form plectonemes and its extension is maximal. If we subsequently modulate F between 1 and 5 pN the molecule is switched between states with and without plectonemes (see Fig. 12). Performing this modulation with and without Topo II leads to a clear signature of the enzyme's binding as seen in Fig. 13. When the force is increased to 5 pN in presence of Topo II, the extension of the molecule is transiently blocked at values smaller than its full extension at this force.
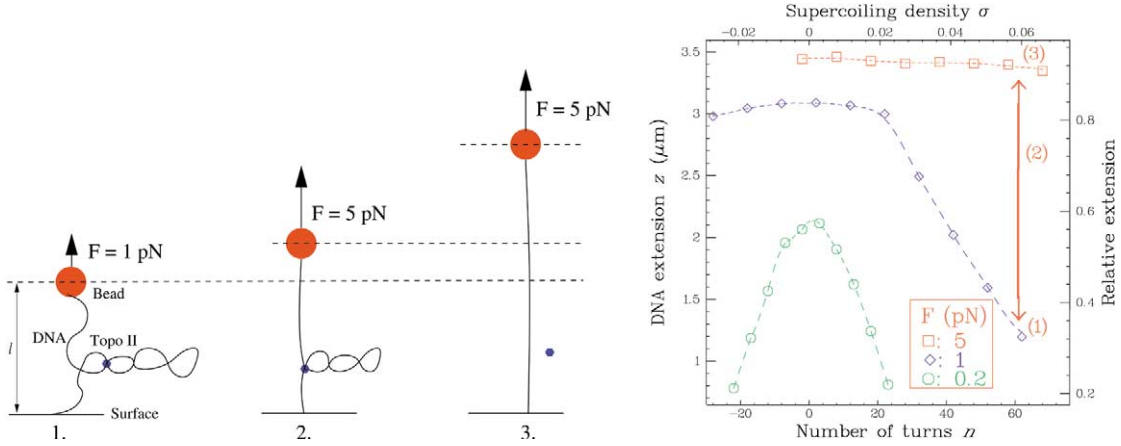
Figure 12. Left: interpretation of the curves in Fig. 13. (1) When a Topo II clamps a crossover between DNA segments, it (2) protects a certain number of plectonemes from a sudden increase in the force. (3) When the enzymatic clamp releases either one or both of the DNA segments, the remaining plectonemes are suddenly exposed to the higher stretching force and rapidly disappear. Right: extension of the DNA molecule versus number of turns applied for 0.2, 1 and 5 pN. This last two values correspond to the forces span by the modulation, the 0.2 pN curve mark the relaxed state of the molecule.
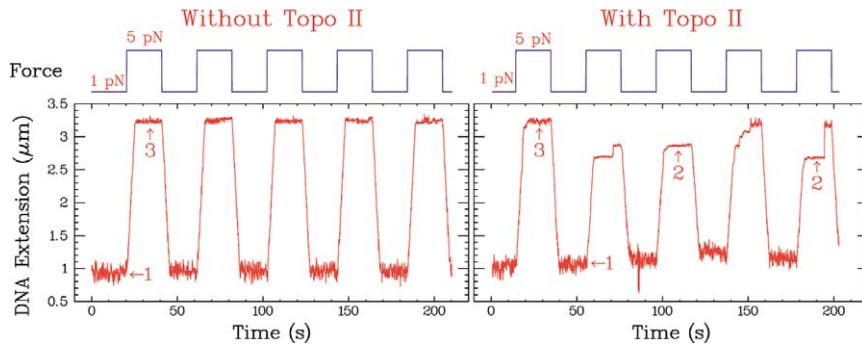

Figure 13. Pulling out plectonemes in the (A) absence or (B) presence of Topo II. The DNA is overwound by $n = 60$ turns and subjected to a force alternating between 1 and 5 pN. In the absence of enzyme, the increase in force removes all the plectonemes, resulting in a progressive increase in the system's extension. In the presence of enzyme, we observe pauses in the system's rise. The end of this pause is marked by a quasi-instantaneous increase in the bead's height.

4.5.2. *Single binding events of Topo II*

In a second binding assay, we set the number of turns n applied to the DNA molecule close to the buckling instability threshold $n \sim n_b$. Unlike the well defined buckling threshold of a rope, the instability for a DNA molecule is smoothed by strong thermal fluctuations. These fluctuations may switch a DNA molecule between a state without plectonemes and a state containing the simplest plectoneme (a single loop of radius R_c). The corresponding length of the DNA molecule thus switches between z_0 (maximal length) and $z_1 = z_0 - 2\pi R_c$. In the absence of Topo II, the switching between these two states is so rapid that the extension measured is an average between z_0 and z_1. However the fluctuations are noticeably modified in the presence of Topo II: as the lifetime of the looping state is significantly increased by the protein binding. The molecule's extension z then displays telegraphic noise, oscillating randomly between z_0 and z_1 (see Fig. 14, $z_0 - z_1 = 40$ nm). The duration of the state with extension z_1 corresponds to the binding lifetime t_{clamp} of the topoisomerase (note that in some rare occasions two loops may be stabilized simultaneously).
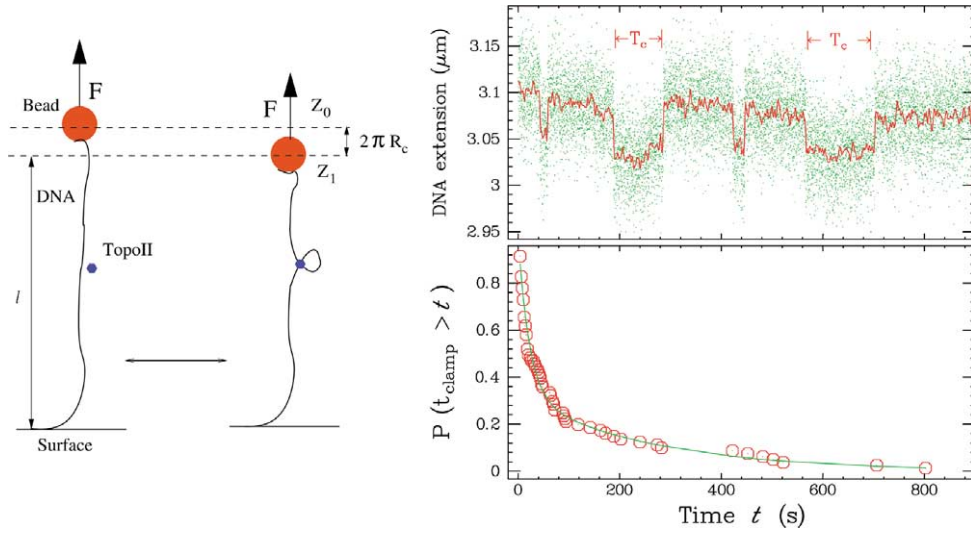
610

Figure 14. Left: experimental strategy allowing us to measure the time during which a Topo II clamps a DNA crossover. The DNA is stretched by a 1 pN force and overwound to the threshold of the buckling instability $n_1 = n_b$. In the absence of Topo II, thermal fluctuations cause one or two loops to appear and disappear at a rate much higher than the temporal and spatial resolution of our system. However, when a Topo II stabilizes one of these loops by crossover clamping, the system's extension decreases by $\delta = 40$ nm, i.e. the size of a loop. The lifetime of this 'contracted' state is sufficiently long for observation. When the enzyme releases the crossover, the system's mean extension increases by $\delta = 40$ nm. The time between the stabilization and the release of the loop directly gives the clamp's lifetime. Right: (top) observation of clamping events in the absence of divalent cation. Although Roca et al. [59] concluded that no clamping took place in these conditions, we see in fact that the enzyme is still capable of forming a ternary complex with DNA. (Bottom) $P(t_{clamp} > t)$ (the integral of the probability distribution of clamp lifetimes) represents the probability that a clamping event will have a lifetime $t_{clamp} > t$ in the presence of Mg^{2+} cations. This probability is well-described by a double-exponential decay (see Section 4.5.2).

We further observed that the kinetics of binding to a DNA crossover strongly depends upon the salt concentration (especially $[Mg^{2+}]$). In the presence of Mg^{2+}, the time distribution presents at least two distinct k_{off} rates: roughly 70% of the clamping events have a half-life of ~ 20 s, while the remaining 30% have a half-life of ~ 260 s (see Fig. 14). When Mg^{2+} is removed, one notes the disappearance of long clamping times.

Such binding events have similarly been observed (indirectly) on long time scales by Roca et al. (in ensemble experiments) [59] and on short time scales by Zechiedrich and Osheroff (using electron microscopy) [58]. In the absence of divalent cations, the ensemble experiments were unable to detect crossover clamping, in contrast to the electron microscopy measurements. The observation of multiple time scales using our single-molecule experiments explain the discrepancy between their observations. These results imply the existence of at least two different configurations for the enzyme/DNA–DNA complex in absence of ATP.

We thus conclude from these binding studies, that Topo II is able to hold the two segments of a DNA firmly for a few seconds before releasing them. This assay demonstrates that Topo II binds to DNA crossings without need of ATP. It also rules out models proposing that the enzyme forms a free sliding loop [45].

4.6. What do we learn about Topo II kinetic cycle?

The preceeding experiments serve to illustrate several aspects of Topo II's interaction with DNA. Ultimately we would like to know whether the model of Fig. 6 correctly describes Topo II activity. Furthermore, what are the chemical constants k_i which characterize each of the sub-cycles of enzyme activity?
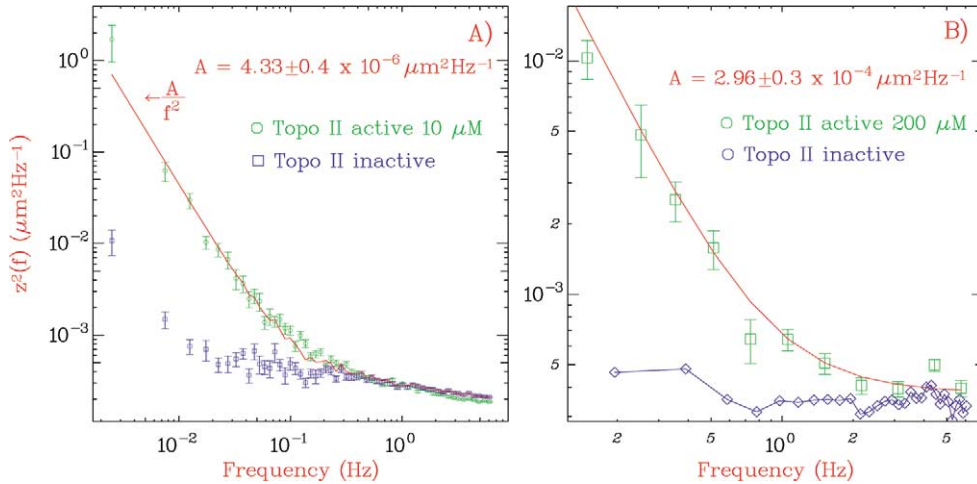
Figure 15. Step distribution analysis of Topo II working at $F = 0.7$ pN and for two different [ATP] concentrations. The average velocity power spectrum of relaxation runs (green) are compared with the experimental noise (blue). (A) [ATP] $= 10$ μM, 17 relaxations runs (green) and 12 experimental noise records (blue). The red curve is a fit to a A/f^2 component added to noise leading to $r = 0.97 \pm 0.1$, knowing that $\epsilon = 86$ nm [57]. At high frequency all curves converge. The quality of the data is sufficient ($Q \sim 50$) to extract steps in real time. (B) At 200 μM ATP, this is no longer the case and data can only be treated in Fourier space (16 active runs compared with 8 inactive one), leading to $r = 0.54 \pm 0.1$.

At present, the different experiments that we have described allow us to partially confirm the model proposed by J. Lindsley [55,56] but some of the values of the associated chemical constants k_i remain known.

In general, the enzymatic turnover time $\propto 1/k$ is a complicated convolution of the individual rate constants k_i. If, however, one sub-cycle is rate-limiting, i.e. if it is much slower than all the others $k_l \gg k_{i \neq l}$, then the enzymatic rate k is nearly equal to k_l. In such a situation, the enzymatic turnover time is described by a Poisson distribution. Acting upon the cofactors involved in the enzymatic reaction is a way to change the limiting sub-cycle. For instance, lowering the ATP concentration slows down the ATP binding sub-cycle, permitting measurement of the ATP binding rate k_a. Alternatively, when we observe that the stretching force F reduces the enzymatic activity, we deduce that an additional rate-limiting step is influenced by the tension on the DNA molecule. In that case we determine a rate k_f, interpreted as the religation rate. Varying the various parameters: ATP concentration, stretching force, temperature, etc., will help us to characterize quantitatively the reaction steps.

The method is developed in Section 2.4.1, to deduce the number of limiting steps and the associated rate constants k_i from the probability distribution of enzymatic activity.

At low ATP concentrations, as already said, steps are clearly identified in the temporal signal and the Fourier analysis is not needed, but confirms the results previously obtained: $r = 1$ (see Fig. 15) so that there is one limiting step (ATP binding) and the distribution of cycle duration is Poissonian. However, at 200 μM ATP, steps cannot be identified in the temporal signal (so that extraction of cycle duration in the time domain is impossible) but frequency analysis of the noise yields to $r = 0.58$ (see Fig. 15). This means that the enzymatic kinetics are sub-Poissonian and that each cycle can be viewed as two consecutive sub-cycles of approximately equal lifetime. What are these kinetic limiting steps? As the concentration of ATP is a bit lower than Km, binding of ATP may still be involved in the limitation of the enzymatic process. The other step might be the release of ADP or phosphate after hydrolysis. Similar analysis have been achieved on molecular motors [17,60–62].

5. Studies of other topoisomerases

We have now shown that DNA micromanipulation is a robust tool for the study of Topo II. We now present a comparison with the activity of the bacterial form of Topo II. This shows that despite their apparent similarity the two enzymes have very different mechanisms of action.

5.1. Topoisomerase IV relaxes positive and negative supercoils with very different rates

The same experiments performed with (prokaryotic) Topo IV yield somewhat different results. Whereas for positive supercoiling, the measured relaxation rate is comparable to that observed on Topo II, the relaxation of negative supercoils is barely visible (see Fig. 16). We observe a slow relaxation of negative supercoiling only when we increase enzyme concentration by a factor 5, suggesting a cooperative mode of action.

For these experiments, the enzyme was at a concentration of 10 ng/ml (30 fM), and only one enzyme acted on the DNA at any given moment, using the single-molecule criterion discussed in Section 4.2. We measured the maximal rate of relaxation of positive supercoils V_{max} by the method described previously. We obtain $V_{max} \sim 3$ cycles/s, very close to the rate observed on Topo II. We note that this value is 1200 times greater than the value obtained by Hiasa et al. [63] (in slightly different ionic conditions).

5.2. Relaxation of negative supercoils by Topo IV

The behavior of Topo IV changes radically when its target DNA is negatively supercoiled, see Fig. 17. Indeed, the relaxation of negative supercoils is only observable once enzyme concentrations exceed 50 ng/ml (150 fM), and does not seem very processive. At this concentration, it is quite likely that multiple enzymes are in interaction with the DNA at any given moment. Moreover, the enzyme does not relax all
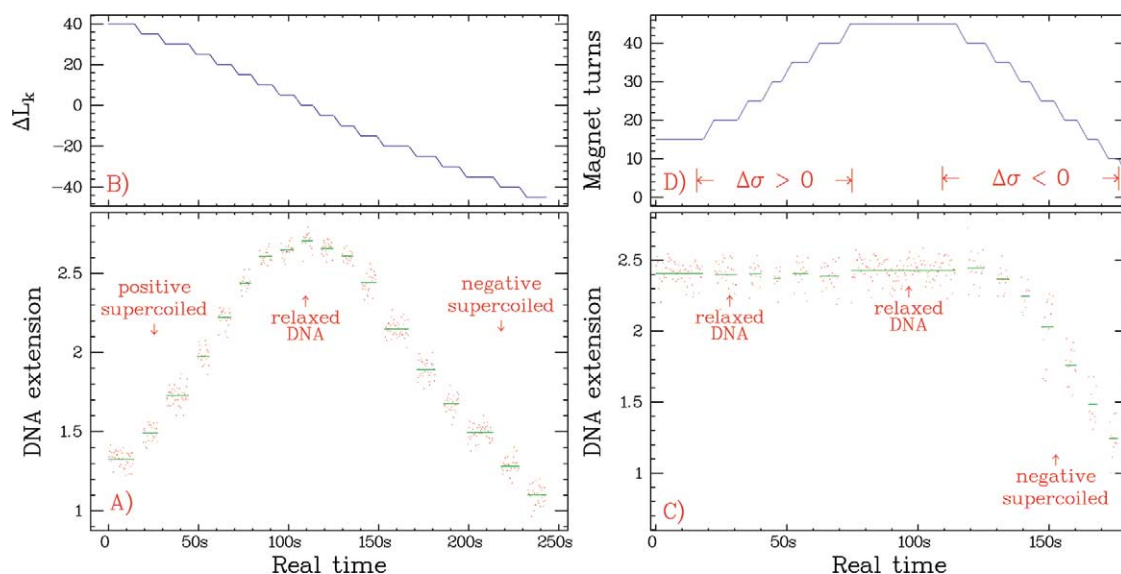

Figure 16. Single-molecule assay of E. coli Topo IV with $F = 0.2$ pN. In (A) and (C) the DNA extension is displayed versus time while the magnets are rotated. In (A) the experiment is performed without enzyme, and thus the DNA extension presents a maximum value when the linking number is null. When turns are added or removed (as shown in (B)), the molecule shrinks due to the formation of plectonemes. When the E. coli Topo IV is added, positively supercoiled DNA is relaxed very efficiently. On the other hand, negative supercoiled is barely relaxed and plectonemes shorten the molecule. The dotted curves in (A) and (C) correspond to a signal averaging over 0.32 second. The steps correspond to the averaged signal over the time period where magnets are stationary.
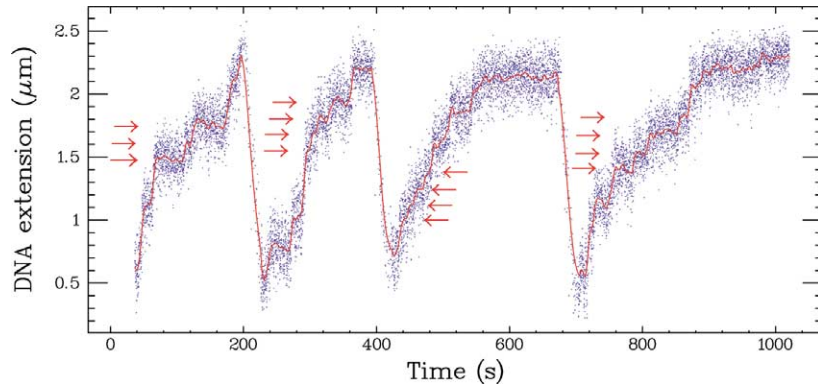
Figure 17. Relaxation of negative supercoils by Topo IV at a concentration of 50 ng/ml. Points correspond to the raw experimental data, and the full line to an averaging over a few seconds. The relaxation is much slower than if the DNA were positively supercoiled. Arrows indicate single cycles which were resolved.
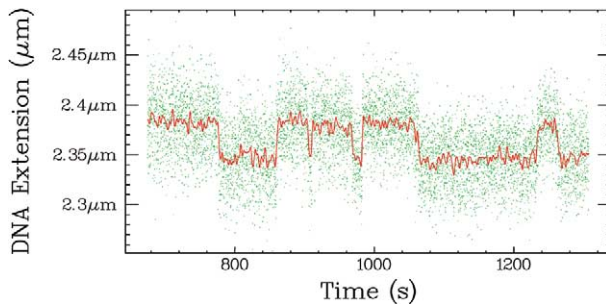

Figure 18. Clamping event observerved with Topo IV in a similar array as described in Fig. 14.

the supercoils ($Wr \neq 0$), as indicated by the fact that the DNA's extension does not recover its maximal value ($l_{\max}$ indicated by the dashed line in Fig. 17). We have verified that this is not due to the appearance of denatured regions in the DNA.

5.3. Topo IV binding events in the absence of ATP

Using Topo IV we have repeated the binding experiments done on Topo II and described in Sections 4.5.1 and 4.5.2. The results are interesting: in contrast to those obtained with Topo II, the yanking assay on Topo IV reveals no binding of the two DNA segments whereas the clamping assay produces the same signal for both enzymes (see Fig. 18). This indicates that binding mechanism is different for the two enzymes. The clamping assay indicates that DNA wraps around Topo IV whereas the absence of yanking signal indicates that the enzyme does not have a firm hold on the two DNA segments. It will be interesting to investigate the underlying differences between the Topo II and Topo IV binding mechanisms in more detail.

5.4. Unresolved questions on topoisomerases

The mode of action of topoisomerases is not yet fully understood, and a very important question remains: how do these small enzymes detect the topological state of the DNA molecule and act in order to relax or simplify its topology? This question is especially delicate since these enzymes have a ~ 5 nm size whereas the topological structure of the DNA extends over large distances. This question poses a real problem exposed by Rybenkov et al. [45]. These authors have shown a strong paradox: whereas Topo I relaxes a supercoiled plasmid population to its expected equilibrium thermodynamic distribution, Topo II and Topo IV relax such a population beyond the thermodynamic equilibrium resembling a Maxwell demon.

No physical laws are violated here since Topo II and Topo IV consume energy (ATP) in the process. Nonetheless, the exact mechanism driving the reaction beyond equilibrium remains unclear. Three models have been proposed so far to explain this mechanism [45,64,65] but no experiment has confirmed or revoked them.

Furthermore, the interplay between various topoisomerases in the cell makes the regulation of DNA topology much more complex: in prokaryotes, DNA is maintained negatively supercoiled by gyrase, a member of the type II topoisomerase family. This enzyme uses the energy of ATP hydrolysis to introduce negative supercoiling into DNA. The overall degree of supercoiling is a delicate balance between gyrase activity and that of other topoisomerases (i.e. Topo I and to some extent Topo IV). The mechanism of the regulation of DNA topology by the local and opposed actions of few enzymes still remains to be fully understood.

6. Conclusion

Using magnetic tweezers, we have studied the enzymatic activity of topoisomerases acting on the DNA molecule. We achieve this goal by micromanipulating the substrate of the enzyme: the DNA molecule. The enzyme is unmodified and thus its biophysical characteristics may be compared with ensemble experiments. In these conditions, we have shown that we recover the results already found in ensemble experiment. Moreover, following the activity in real-time gives access to the biochemical constants involved in the enzyme cycle. This improved knowledge is not only of purely academic interest: blocking the cycle of topoisomerases is lethal for the cell and topoisomerase inhibitors are massively used either as antibiotics or in anti-cancer treatment (chemotherapy). A better understanding of enzyme mechanisms is thus of particular importance, and we have illustrated here that single-molecule experiments bring new insights to these issues. Furthermore, they give a fascinating picture of enzymes working as impressive nano-machines performing significant structural changes. The versatile micromanipulation techniques offer the ability to mechanically act upon the enzyme. Bridging the macroscopic and nanoscopic world, the experimentalist is now able to slow down an enzyme by pulling on the DNA leash.

Appendix A

A.1. Topo II experimental conditions

The Topo II experiments were performed with *D. melanogaster* Topo II at 25 °C in the ionic conditions described by [59]: 50 mM Tris (pH 8) containing 50 mM KCl, 8 mM $MgCl_2$, 1 mM EDTA, 0.2% Tween-20, 0.5 mM DTT and 200 µg/ml BSA.

A.2. Topo IV experimental conditions

Here we assayed it at 25 °C in a 25 mM Tris buffer (pH 7.6) containing 100 mM KGlutamate, 10 mM $MgCl_2$, 0.5 mM DTT, 50 µg/ml BSA and 0.1% Triton X-100. The applied stretching force was $F = 0.2$ pN, and the experiments were performed in the presence of 1 mM ATP.

A.3. Characterization of enzymatic activity in the time domain

Frequency analysis is extremely powerful but often one wants to pinpoint the individual steps of an enzymatic cycle. If the signal is large enough compared to the experimental noise ($Q > N$), the enzyme's steps can be isolated from the temporal signal. As signal and noise are indistinguishable above the characteristic frequency f_c, that frequency corresponds to the optimum averaging time $t_c = 2\pi/f_c$ that has to be used to extract the steps in the time domain. Using a smaller averaging time decreases the signal to noise ratio while a larger one results in a smearing of the step profile.

Now that we have defined the best averaging time, we must find the position and size of the steps which is still not a easy task. We propose here a simple algorithm that gives good results and provides a criterion that may be used to control the result. We assume that the signal is sampled regularly in time with a period T_e small enough to capture the relevant information. Thus our signal is a discrete series of data points. The principle that we have used consists in applying a sliding window to the signal with a typical width $t_{av} = 2t_c$ corresponding to a discrete number of points n_{av}. In that window, we assume that a single step is present and thus fit the signal $z(t)$ to a Heaviside function equals to z_0 at the beginning of the window and z_1 at the end. The position of the step t_s inside the window is allowed to vary from $t_0 + t_{av}/4$ to $t_0 + 3t_{av}/4$. The step levels z_0 and z_1 correspond to the signal respectively averaged over $[t_0, t_s]$ and $[t_s, t_1]$. t_s is selected to correspond to one of the sampling point times such as to minimize the variance of the signal minus this z_0, z_1 step (χ^2 minimization):

$$\chi^2(t_s) = \sum_{\substack{t_i = t_0}}^{t_i < t_s} \left(z(t_i) - z_0 \right)^2 + \sum_{\substack{t_i = t_s}}^{t_i < t_0 + t_{av}} \left(z(t_i) - z_1 \right)^2 \tag{8}$$

$$\text{with} \quad z_0 = \sum_{\substack{t_i = t_0}}^{t_i < t_0 + t_s} z(t_i) \Bigg/ \left(\sum_{\substack{t_i = t_0}}^{t_i < t_0 + t_s} \right) \quad \text{and} \quad z_1 = \sum_{\substack{t_i = t_0 + t_s}}^{t_i < t_0 + t_{av}} z(t_i) \Bigg/ \left(\sum_{\substack{t_i = t_0 + t_s}}^{t_i < t_0 + t_{av}} \right).$$

This algorithm will find a step in every window regardless of the nature of the signal. We now need a method to characterize the relevance of the steps thus determined. Let us first define the maximum number of observable steps $N_{max} = T/t_c$. By moving the window along the data signal for every sample, we record the position t_s and size $\delta z = z_1 - z_0$ for all time data (that is for each sample of signal). Imagine that a real step is located at t_r, we shall find that when the window slides from $t_0 = t_r - 3t_c/4$ till $t_0 = t_r - t_c/4$, the t_s found by minimizing χ^2 is such that t_s is very close to t_r for a number of points corresponding to $n_{av}/2$. If only noise is present, t_s will vary as the averaging window is sled. By constructing an histogram of the positions t_s we select those that are peaked around a fixed value scoring a number close to $n_{av}/2$ which most probably correspond to real steps.

This simple algorithm works reasonably well as may be seen on Fig. 11. The best way to characterize the inherent noise in this method is to apply it to a stretch experimental noise and to determine the variance of the step size. Notice also that by construction, the method is blind to steps shorter than the averaging window.

References

[1] K. Svoboda, C.F. Schmidt, B.J. Schnapp, S.M. Block, Direct observation of kinesin stepping by optical trapping interferometry, Nature 365 (1993) 721–727.

[2] J.T. Finer, R.M. Simmons, J.A. Spudich, Single myosin molecule mechanics: piconewton forces and nanometre steps, Nature 368 (1994) 113–119.

[3] H. Noji, R. Yasuda, M. Yoshida, K. Kinosita, Direct observation of the rotation of F_1-ATPase, Nature 386 (1997) 299–302.

[4] J.-F. Allemand, D. Bensimon, V. Croquette, R. Lavery, B. Maier, T. Strick, Le jokari moléculaire, Biofutur 190 (1999) 26–30.

[5] E.L. Florin, V.T. Moy, H.E. Gaub, Adhesion force between individual ligand-receptor pairs, Science 264 (1994) 415–417.

[6] F. Oesterhelt, D. Oesterhelt, M. Pfeiffer, A. Engel, H.E. Gaub, D.J. Müller, Unfolding pathways of individual bacteriorhodopsins, Science 286 (2000) 143–146.

[7] A. Ashkin, Applications of laser radiation pressure, Science 210 (1980) 1081–1088.

[8] A. Ashkin, K. Schütze, J.M. Dziedzic, U. Eutenauer, M. Schliwa, Force generation of organelle transport measured *in vivo* by an infrared laser trap, Nature 348 (1990) 346–348.

[9] K. Svoboda, S. Block, Biological applications of optical forces, Annu. Rev. Biophys. Biomol. Struct. 23 (1994) 247–285.

[10] E. Evans, K. Ritchie, R. Merkel, Sensitive force technique to probe molecular adhesion and structural linkages at biological interfaces, Biophys. J. 68 (1995) 2580–2587.

[11] R. Merkel, P. Nassoy, A. Leung, K. Ritchie, E. Evans, Energy landscapes of receptor-ligand bonds explored with dynamic force spectroscopy, Nature 397 (1997) 50–53.

[12] S.B. Smith, L. Finzi, C. Bustamante, Direct mechanical measurements of the elasticity of single DNA molecules by using magnetic beads, Science 258 (1992) 1122–1126.

[13] R. Lavery, A. Lebrun, J.-F. Allemand, D. Bensimon, V. Croquette, Structure and mechanics of single biomolecules: Experiment and simulation, J. Phys. Condens. Matter 14 (2002) R383–R414.

[14] T. Strick, J.F. Allemand, D. Bensimon, A. Bensimon, V. Croquette, The elasticity of a single supercoiled DNA molecule, Science 271 (1996) 1835–1837.

[15] T. Strick, J.-F. Allemand, D. Bensimon, V. Croquette, The behavior of supercoiled DNA, Biophys. J. 74 (1998) 2016–2028.

[16] C. Gosse, V. Croquette, Magnetic tweezers: micromanipulation and force measurement at the molecular level, Biophys. J. (2002), to appear in June.

[17] K. Visscher, M.J. Schnitzer, S.M. Block, Single kinesin molecules studied with a molecular force clamp, Nature 400 (1999) 184–189.

[18] R. Yasuda, H. Noji, K. Kinosita, M. Yoshida, F_1-ATPase is a highly efficient molecular motor that rotates with discrete 120° steps, Cell 93 (1998) 1117–1124.

[19] G. Charvin, D. Bensimon, V. Croquette, On the relation between noise spectra and the distribution of time between steps for single molecular motors, Single Mol. 3 (2002) 43–48.

[20] M.J. Schnitzer, S.M. Block, Statistical kinetics of processive enzymes, in: Cold Spring Harbor Symposia on Quantitative Biology, Vol. LX, 1995, pp. 793–801.

[21] J.F. Marko, E.D. Siggia, Fluctuations and supercoiling of DNA, Science 265 (1994) 506–508.

[22] C. Bouchiat, M.D. Wang, S.M. Block, J.-F. Allemand, T.R. Strick, V. Croquette, Estimating the persistence length of a Worm-Like Chain molecule from force-extension measurements, Biophys. J. 76 (1999) 409–413.

[23] P. Cluzel, A. Lebrun, C. Heller, R. Lavery, J.-L. Viovy, D. Chatenay, F. Caron, DNA: an extensible molecule, Science 271 (1996) 792–794.

[24] S.B. Smith, Y. Cui, C. Bustamante, Overstretching B-DNA: the elastic response of individual double-stranded and single-stranded DNA molecules, Science 271 (1996) 795–799.

[25] T.C. Boles, J.H. White, M.R. Cozzarelli, Structure of plectonemically supercoiled DNA, J. Mol. Biol. 213 (1990) 931–951.

[26] J. Bednar, P. Furrer, A. Stasiak, J. Dubochet, E. Egelman, A. BatetSrich, The twist, writhe and overall shape of supercoiled DNA change during couterion-induced transition from a loosely to a tightly interwound superhelix, J. Mol. Biol. 235 (1994) 825–847.

[27] J.H. White, Self linking and the Gauss integral in higher dimensions, Amer. J. Math. 91 (1969) 693–728.

[28] C.R. Calladine, H.R. Drew, Understanding DNA, Academic Press, 1992.

[29] T. Strick, V. Croquette, D. Bensimon, Homologous pairing in streched supercoiled DNA, Proc. Natl. Acad. Sci. USA 95 (1998) 10579–10583.

[30] J.-F. Allemand, D. Bensimon, R. Lavery, V. Croquette, Stretched and overwound DNA forms a Pauling-like structure with exposed bases, Proc. Natl. Acad. Sci. USA 95 (1998) 14152–14157.

[31] J.F. Marko, E. Siggia, Statistical mechanics of supercoiled DNA, Phys. Rev. E 52 (3) (1995) 2912–2938.

[32] C. Bouchiat, M. Mézard, Elasticity theory of a supercoiled DNA molecules, Phys. Rev. Lett. 80 (1998) 1556–1559.

[33] C. Bouchiat, M. Mézard, Elasticity rod model of supercoiled DNA molecules, cond-mat/9904018, 1999.

[34] J.D. Moroz, P. Nelson, Torsional directed walks, entropic elasticity and DNA twist stiffness, Proc. Natl. Acad. Sci. USA 94 (1998) 14418–14422.

[35] J.D. Moroz, P. Nelson, Entropic elasticity of twist-storing polymers, Macromolecules 31 (1998) 6333–6347.

[36] T.R. Strick, J.-F. Allemand, D. Bensimon, V. Croquette, Stress induced structural transitions in DNA and proteins, Annu. Rev. Biophys. Biomol. Struct. 29 (2000) 523–540.

[37] J.F. Léger, G. Romano, A. Sarkar, J. Robert, L. Bourdieu, D. Chatenay, J.F. Marko, Structural transitions of a twisted and stretched DNA molecule, Phys. Rev. Lett. 83 (1999) 1066–1069.

[38] J.M. Berger, S.J. Gamblin, S.C. Harrison, J.C. Wang, Structure and mechanism of DNA topoisomerase II, Nature 379 (1996) 225–232.

[39] J.D. Watson, F.H.C. Crick, Molecular structure of nucleic acids: a structure for deoxyribose nucleic acid, Nature 171 (1953) 737–738.

[40] J.C. Wang, Interaction between DNA and an *escherichia coli* protein ω, J. Mol. Biol. 55 (1971) 523–533.

[41] L.F. Liu, C.C. Liu, B.M. Alberts, Type II DNA topoisomerases: enzymes that can unknot a topologically knotted DNA molecule via a reversible double-stranded break, Cell 19 (1980) 697–707.

[42] T. Hsieh, Knotting of the circular duplex DNA by type II DNA topoisomerase from *drosophila melanogaster*, J. Biol. Chem. 258 (1983) 8413–8420.

[43] J. Roca, J.C. Wang, The capture of a DNA double helix by an ATP-dependent protein clamp: a key step in DNA transport by type II DNA topoisomerase, Cell 71 (1992) 833–840.

[44] J. Roca, J.M. Berger, S.C. Harrison, J.C. Wang, DNA transport by a type II topoisomerase: Direct evidence for a two-gate mechanism, Proc. Natl. Acad. Sci. USA 93 (1996) 4057–4062.

[45] V.V. Rybenkov, C. Ullsperger, A.V. Vologodskii, N.R. Cozzarelli, Simplification of DNA topology below equilibrium values by type II topoisomerases, Science 277 (1997) 690–693.

[46] K. Kirkegaard, J.C. Wang, Bacterial DNA topoisomerase I can relax positively supercoiled DNA containing a single-stranded loop, J. Mol. Biol. 185 (1985) 625–637.

[47] M. Drolet, X. Bi, L.F. Liu, Hypernegative supercoiling of the DNA template during trancription elongation *in vitro*, J. Biol. Chem. 269 (1994) 2068–2074.

[48] E. Masse, Relaxation of transcription-driven negative supercoils is an essential function of *e. coli* topoisomerase I, J. Biol. Chem. 274 (1999) 16654–16658.

[49] E. Masse, *E. coli* DNA topoisomerase I inhibits R-loop formation by relaxing transcription-induced negative supercoils, J. Biol. Chem. 274 (1999) 16659–16664.

[50] M.D. Wang, M.J. Schnitzer, H. Yin, R. Landick, J. Gelles, S. Block, Force and velocity measured for single molecules of RNA polymerase, Science 282 (1998) 902–907.

[51] N. Osheroff, E.R. Shelton, D.L. Brutlag, DNA topoisomerase II from *drosophila melanogaster*: relaxation of supercoiled DNA, J. Biol. Chem. 258 (1983) 9536–9543.

[52] N. Crisona, T.R. Strick, D. Bensimon, V. Croquette, N. Cozzarelli, Preferential relaxation of positively supercoiled DNA by E.coli topoisomerase VI in single-molecule and ensemble measurements, Genes Developement 14 (2000) 2881–2892.

[53] M.D. Wang, M.J. Schnitzer, H. Yin, R. Landick, J. Gelles, S.M. Block, Force and velocity measured for single molecules of RNA polymerase, Science 282 (1998) 902–907.

[54] W. Hua, E.C. Young, M.L. Fleming, J. Gelles, Coupling of kinesin steps to ATP hydrolysis, Nature 388 (1997) 390–393.

[55] T.T. Harkins, J.E. Lindsley, Pre-steady-state analysis of ATP hydrolysis by *saccharomyces cerevisiae* DNA topoisomerase II. 1. A DNA-dependent burst in ATP hydrolysis, Biochemistry 37 (1998) 7292–7298.

[56] T.T. Harkins, T.J. Lewis, J.E. Lindsley, Pre-steady-state analysis of ATP hydrolysis by *saccharomyces cerevisiae* DNA topoisomerase II. 2. Kinetic mechanism for the sequential hydrolysis of two ATP, Biochemistry 37 (1998) 7299–7312.

[57] T. Strick, J.-F. Allemand, D. Bensimon, R. Lavery, V. Croquette, Phase coexistence in a single DNA molecule, Physica A 263 (1999) 392–404.

[58] E.L. Zechiedrich, N. Osheroff, Eukaryotic topoisomerases recognize nucleic acid topology by preferentially interacting with DNA crossovers, EMBO J. 9 (1990) 4555–4562.

[59] J. Roca, J.M. Berger, J.C. Wang, On the simultaneous binding of eukaryotic DNA topoisomerase II to a pair of double-stranded DNA helices, J. Biol. Chem. 268 (1993) 14250–14255.

[60] M.J. Schnitzer, S.M. Block, Kinesin hydrolyses one ATP per 8-nm step, Nature 388 (1997) 386–390.

[61] M. Rief, R.S. Rock, A.D. Mehta, M.S. Mooseker, R.E. Cheney, J.A. Spudich, Myosin-v stepping kinetics: A molecular model for processivity, Proc. Natl. Acad. Sci. USA 97 (17) (2000) 9482–9486.

[62] R.S. Rock, S.E. Rice, A.L. Wells, T.J. Purcell, J.A. Spudich, H.L. Sweeney, Myosin vi is a processive motor with a large step size, Proc. Natl. Acad. Sci. USA 98 (24) (2001) 13655–13659.

[63] H. Hiasa, K.J. Marians, Two distinct modes of strand unlinking during θ-type DNA replication, J. Biol. Chem. 271 (1996) 21529–21535.

[64] J. Yan, M.O. Magnasco, J.F. Marko, Kinetic proofreading mechanism for disentanglement of DNA by topoisomerases, Nature 401 (1999) 932–935.

[65] A.V. Vologodskii, W. Zhang, D. Subramanian, V.V. Rybenkov, D. Griffith, N.C. Cozzarelli, Mechanism of topology simplification by type II DNA topoisomerases, Proc. Natl. Acad. Sci. USA 98 (2001) 3045–3049.